IEEE Access
Multidisciplinary ⋮ Rapid Review ⋮ Open Access Journal

Received 5 March 2024, accepted 18 March 2024, date of publication 25 March 2024, date of current version 3 April 2024.

Digital Object Identifier 10.1109/ACCESS.2024.3381501

RESEARCH ARTICLE

Low Complexity Hybrid-Field Channel Estimation Based on Simultaneous Weighted OMP Algorithm in Extreme Large-Scale MIMO Systems

HUAN HUANG[1,2], JUNXIN ZHANG[1,2], AND JUN JIANG[1,2,3]
[1]College of Information Science and Technology, Tibet University, Lhasa 850000, China
[2]Information Technology National Experimental Teaching Demonstration Center, Tibet University, Lhasa 850000, China
[3]Tibetan Information Technology Engineering Research Center, Ministry of Education, Tibet University, Lhasa 850000, China

Corresponding author: Jun Jiang (jiangjun9902@utibet.edu.cn)

This work was supported in part by the National Natural Science Foundation of China under Grant 62261051.

ABSTRACT Extreme large-scale multiple-input multiple-output (XL-MIMO) is one of the key technologies for future 6G communications. Channel estimation plays a crucial role in XL-MIMO systems, as accurate Channel State Information (CSI) is essential for effective signal transmission. The existing channel estimation methods mainly distinguish between far-field channel estimation and near-field channel estimation. In the case where the sparsity of the channel is known, the traditional Orthogonal Matching Pursuit (OMP) algorithm is relied upon to estimate the hybrid-field channel in XL-MIMO systems.To overcome these limitations, in this paper, we propose a joint hybrid-field channel estimation scheme and adopt the Simultaneous Weighted Orthogonal Matching Pursuit (SWOMP) algorithm to effectively address these issues. Specifically, to more effectively estimate the hybrid-field channel, we propose a joint channel estimation approach that no longer distinguishes between far-field and near-field channel estimation methods. In the case where the sparsity of the hybrid-field channel is unknown, we employ the SWOMP algorithm to accurately estimate the channel state information. Furthermore, we substitute the Sherman-Morrison-Woodbury transform for the matrix inversion operation in the SWOMP algorithm, which does not reduce computational complexity but provides a novel approach to matrix inversion. Based on this, finally, we further propose a low-complexity SWOMP algorithm based on the Gauss-Seidel method transformation. Simulation results demonstrate that the proposed approach can obtain more accurate channel state information compared to traditional methods in XL-MIMO systems.

INDEX TERMS Extreme large-scale multiple-input multiple-output, channel estimation, hybrid-field, low-complexity simultaneous weighted orthogonal matching pursuit.

I. INTRODUCTION

With the rapid development of communication technology, 6G is expected to achieve ten times the throughput of 5G [1], [2]. One promising technology to achieve this goal is the use of Extremely Large-scale Multiple Input Multiple Output (XL-MIMO) systems. By deploying base stations (BS) with a large number of antennas, XL-MIMO can greatly enhance spectral efficiency and system gain [3], [4]. However, the increase in the number of BS antennas may also lead to an increase in pilot overhead, which could have a negative impact on communication efficiency. Therefore, reducing pilot overhead in XL-MIMO communication networks and obtaining accurate Channel State Information (CSI) using low-complexity algorithms are crucial.

However, due to the deployment of high-frequency radio frequency (RF) links on BS and the potential for high power consumption, a hybrid precoding architecture has been

The associate editor coordinating the review of this manuscript and approving it for publication was Barbara Masini.

© 2024 The Authors. This work is licensed under a Creative Commons Attribution 4.0 License.
For more information, see https://creativecommons.org/licenses/by/4.0/

proposed for BS, which may pose challenges for RF chains with fewer antennas than BS [5]. Additionally, introducing BS's RF links can effectively reduce the pilot overhead for channel estimation. Channel estimation methods based on CS not only reduce pilot overhead but also achieve higher accuracy in sparse channel estimation. For example, in [6], the sparse characteristics of far-field channels in Massive MIMO systems are utilized in the angular domain, and an algorithm based on Compressed Sensing (CS) is used to obtain accurate CSI. As the Message Passing (MP) based CS algorithm requires strict prior distribution of the channel, there are some limitations for channel estimation or signal detection. However, compared to some existing works on sparse channel estimation and signal detection, MP algorithm can achieve higher accuracy with fewer pilot training symbols [7], [8].

In recent years, notable progress has been made in the theory of near-field communication. In [9], it is observed that the sparse characteristics of far-field angle-domain channels are no longer applicable to near-field channels, which may result in greater energy leakage. Therefore, further accurate description of the sparse characteristics of near-field channels is needed to apply CS-based algorithms to near-field channel estimation. In [10], the sparse nature of near-field channels is accurately represented using polar coordinate domain matrices, and the Simultaneous Orthogonal Matching Pursuit (SOMP) algorithm is used to reduce pilot overhead, followed by the deployment of the Simultaneous Iterative Gridless Weighting (SIWG) algorithm to further improve the accuracy of XL-MIMO channel estimation. In [11], the combination of Terahertz (THz) communication with near-field communication is proposed to achieve larger system capacity [12]. Based on the beam splitting effect of Terahertz communication, a method based on bilinear pattern detection is proposed to effectively obtain accurate channel state information. In [13], the authors utilize Reconfigurable Intelligent Surfaces (RIS) to assist near-field communication, which can still achieve reliable communication and improve system throughput even in the presence of obstruction.

When considering the existing scattering situations, it is necessary to simultaneously consider the characteristics of near-field and far-field channels in the communication environment. Therefore, the concept of hybrid-field channels is proposed in XL-MIMO communication systems. Subsequently, some domestic and international articles have conducted research based on literature [14]. In [15], the authors propose a compressed sensing hybrid-field channel estimation algorithm based on the Alternating Directions Method of Multiplier (ADMM), which can effectively reduce the pilot overhead for system channel estimation. In [16], the authors propose to estimate the information brought by the positions of near-field and far-field scattering bodies based on the position information of these bodies, transforming the channel estimation problem into the estimation of parameters for estimating the position of scattering bodies, and similarly achieve good estimation of hybrid-field channel state information. In [17], the authors propose a hybrid-field channel estimation scheme based on changing the deployment of base station antennas and introduce the Support Detection OMP (SD-OMP) algorithm, which can reduce the pilot overhead and improve system spectral efficiency in hybrid-field channel estimation. However, the algorithm proposed in literature [14] needs to distinguish between near-field and far-field for channel estimation, requiring a higher number of pilots, does not achieve efficient channel estimation, and also requires knowledge of channel sparsity, resulting in high algorithm complexity.

Therefore, based on these reasons, this paper considers an XL-MIMO system [18] based on RF chain architecture, which can reduce pilot overhead. In addition, the channel estimation scheme based on [14], [15], and [17] proposes estimating the far-field first and then the near-field in a hybrid-field channel. However, such a scheme is not efficient.Therefore, a joint near-far field channel estimation scheme is proposed to achieve more efficient results. To our knowledge, the need for only one hybrid-field channel estimation without requiring separate coarse and fine estimation schemes is a concept we pioneered. Furthermore, The simultaneous weighted orthogonal matching pursuit algorithm (SWOMP) [19] is used to estimate the channel values even in unknown hybrid-field channel sparsity. Then, based on the ''Woodbury'' transformation [20], the matrix inversion operation in the SWOMP algorithm is replaced to matrix inverse operation. However, the computation complexity did not reduce after the transformation, thus another method based on the ''Gauss-Seidel'' method [21] was proposed to decrease the computation complexity of the algorithm. The main contributions are summarized as follows:

- A joint estimation scheme that does not distinguish between near and far field channels is proposed, which achieves more efficient results in high-dimensional hybrid-field channels. The SWOMP algorithm is then proposed for the joint channel estimation problem, which can still obtain good channel estimation results even in unknown hybrid-field channel sparsity.
- Due to the matrix inversion operation in the SWOMP algorithm, the ''Woodbury'' transformation method is used to replace the matrix inversion step in the algorithm. However, the ''Woodbury'' transformation did not reduce the computation complexity of matrix inversion in the SWOMP algorithm, so a method based on the ''Gauss-Seidel'' method is proposed to reduce the computation complexity of matrix inversion in the SWOMP algorithm to a linear computation complexity.
- Finally,simulation results are presented to demonstrate its effectiveness and superiority over existing algorithms in terms of reduced complexity without sacrificing performance.

The remaining parts of this article are arranged as follows. Part 2 introduces the system model, where the channel model of hybrid-field is described in detail, and the angle

domain matrix that makes the far-field channel sparse and the polarization domain matrix that makes the near-field channel sparse are characterized. In Part 3, the joint channel estimation problem is formulated, and a channel estimation algorithm is proposed. Part 4 followed by an equivalent replacement method for the matrix inversion process in the algorithm. Part 5 proposes a low-complexity algorithm based on matrix inversion, and its convergence is analyzed. Simulation results to verify the effectiveness of the proposed algorithm are presented in Part 6, and Part 7 concludes this paper.

II. SYSTEM MODEL

As shown in Figure 1, the XL-MIMO system based on a hybrid precoding architecture with N_{RF} radio frequency (RF) is considered, and a hybrid-field channel is employed in the Time Division Duplexing (TDD) mode [22]. It is assumed that there are N antennas deployed at the base station (BS) and single antenna deployed at the user equipment (UEs). We consider the uplink communication between the UEs and the BS. Since the channel state information of each user can be obtained individually by K UEs, the channel estimation process typically discusses the channel estimation of any user here.

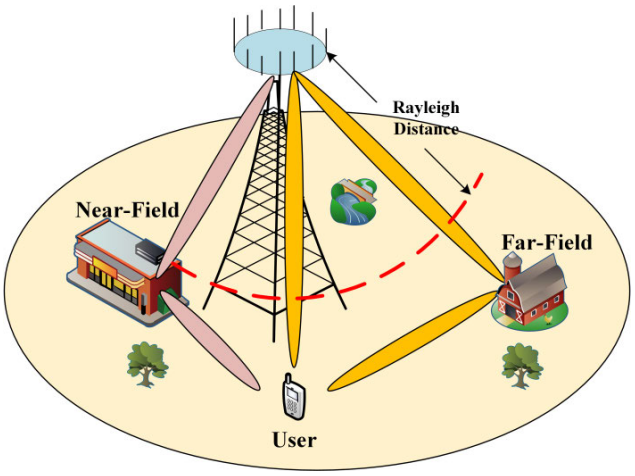

FIGURE 1. Hybrid-field communication scenario of XL-MIMO.

A. SIGNAL MODEL

Specifically, let $\mathbf{h} \in \mathbb{C}^{N\times 1}$ represent the link from a single user to the BS. Let $s(t)$, $\mathbf{w}(t) \in \mathbb{C}^{N\times 1}$, and $\tilde{\mathbf{F}}(t)$ represent the data symbols transmitted to the user in the $t-$th time slot, and the complex Gaussian noise corresponds to the distribution $\mathcal{CN}(0, \sigma_0^2\mathbf{I}_N)$. Therefore, the received signal at the BS can be expressed as:

$$y_t = \tilde{\mathbf{F}}(t)\mathbf{h}s(t) + \tilde{\mathbf{F}}(t)\mathbf{w}(t). \tag{1}$$

Without loss of generality, we assume that $s(t) = 1$, where $t = 1, \cdots, \tau$. The analog value $\mathbf{y}$ received at the BS over the entire τ time slots can be expressed as:

$$\mathbf{y} = \tilde{\mathbf{F}}\mathbf{h} + \mathbf{w}, \tag{2}$$

where $\mathbf{y} = \left[y_1^T, y_2^T, \cdots, y_\tau^T\right]^T \in \mathbb{C}^{\tau N_{RF}\times 1}$和$\mathbf{w} = \left[\mathbf{w}^T(1)\mathbf{F}^T(1), \mathbf{w}^T(2)\mathbf{F}^T(2), \cdots, \mathbf{w}^T(\tau)\mathbf{F}^T(\tau)\right]^T \in \mathbb{C}^{\tau N_{RF}\times 1}$. Let $\tilde{\mathbf{F}} = \left[\tilde{\mathbf{F}^T}(1), \tilde{\mathbf{F}^T}(2), \cdots, \tilde{\mathbf{F}^T}(\tau)\right]^T \in \mathbb{C}^{\tau N_{RF}\times N}$ be the observation matrix, where each element of $\tilde{\mathbf{F}}$ follows the distribution $\frac{1}{\sqrt{N}}\{-1, 1\}$.

Upon observing (2), we note that the noise w is not Gaussian white noise. To accurately obtain CSI, measures should be taken to restore the original noise by pre-whitening. We Let $\mathbf{C} = \sigma_0^2 \text{diag}\{\tilde{\mathbf{F}}(1)\tilde{\mathbf{F}}^H(1), \tilde{\mathbf{F}}(2)\tilde{\mathbf{F}}^H(2), \cdots, \tilde{\mathbf{F}}(\tau)\tilde{\mathbf{F}}^H(\tau)\}$ represent the covariance matrix of $\mathbf{w}$, and use the matrix $\mathbf{G} \in \mathbb{C}^{\tau N_{RF}\times \tau N_{RF}}$ to predict the received signal. The matrix $\mathbf{G}$ is obtained by performing eigenvalue decomposition on $\mathbf{C} = \sigma_0^2\mathbf{V}\mathbf{\Sigma}\mathbf{V}^H$, where $\mathbf{G}=\mathbf{V}\mathbf{\Sigma}^{\frac{1}{2}}$. Multiplying both sides of (2) by $\mathbf{G}$ yields:

$$\overline{\mathbf{y}} = \mathbf{G}^{-1}\mathbf{y} = \mathbf{G}^{-1}\tilde{\mathbf{F}}\mathbf{h} + \mathbf{G}^{-1}\mathbf{w} = \mathbf{\Phi}\mathrm{h} + \overline{\mathbf{w}} \tag{3}$$

where $\mathbf{\Phi} = \mathbf{G}^{-1}\mathbf{F}$ and $\overline{\mathbf{w}} = \mathbf{G}^{-1}\mathbf{w}$. Meanwhile, the noise $\overline{\mathbf{w}} \backsim \mathcal{CN}(0, \sigma_0^2\mathbf{I}_\tau N_R^F)$. The proof is as follows:

$$\begin{aligned}\tilde{\mathbf{C}} &= \mathbb{E}\left[\mathbf{G}^{-1}\mathbf{w}\mathbf{w}^H\mathbf{G}^{-H}\right] \\ &= \mathbb{E}\left[\mathbf{G}^{-1}\mathbf{C}\mathbf{G}^{-H}\right] \\ &= \sigma_0^2\mathbf{\Sigma}^{-\frac{1}{2}}\mathbf{V}^{-1}\mathbf{V}\mathbf{\Sigma}\mathbf{V}^H\mathbf{V}^{-H}\mathbf{\Sigma}^{-\frac{1}{2}} \\ &= \sigma_0^2\mathbf{I}_{\tau N_{RF}},\end{aligned} \tag{4}$$

where $\tilde{\mathbf{C}}$ represents the covariance matrix of the noise $\overline{\mathbf{w}}$.

B. CHANNEL MODEL

In the literatur [14], the concept of a hybrid-field channel is proposed. Therefore, there is no detailed description here. We mainly describe how Rayleigh distance, far-field channel, and near-field channel are modeled. Therefore, the expression for the Rayleigh distance is given as follows:

$$R = \frac{2\overline{D^2}}{\lambda}, \tag{5}$$

where $\overline{D}$ represents the aperture of the antenna array and λ represents the wavelength. It is worth noting that in wireless communication systems, the electromagnetic radiation field may be divided into the far field and near field, resulting in both far-field channels and near-field channels in the communication environment. Specifically, we first introduce the Rayleigh distance in Equation (5), where communication is in the far-field range when $\tilde{d} > R$ and in the near-field range when $\tilde{d} < R$, with $\tilde{d}$ representing the physical distance from the base station to the scatterer. Subsequently, during communication between the user and the base station, in the NLoS path component, the user receives signals after reflections from scatterers in both far-field and near-field

ranges. Therefore, the signal traverses a combination of far-field and near-field channels, referred to as a hybrid-field channel.

The far-field channel $\mathbf{h}_{FF}$ can be modeled as:

$$\mathbf{h}_{FF} = \sqrt{\frac{N}{P}} \sum_{p_f=1}^{P_F} \gamma_{p_f} \mathbf{a}(\theta_{p_f}), \tag{6}$$

where P and P_F respectively represent the total number of paths for the hybrid-field and far-field channels. γ_{p_f} represents the path gain of the p_f-th far-field path, θ_{p_f} represents the angle of the p_f-th far-field path. $\mathbf{a}(\theta_{p_f}) \in \mathbb{C}^{N\times 1}$ is the steering vector of the far-field array, and the expression for $\mathbf{a}(\theta_{p_f})$ is:

$$\mathbf{a}(\theta_{p_f}) = \frac{1}{\sqrt{N}} \left[1, e^{-j2\pi\theta_{p_f}}, \cdots, e^{-j2\pi(N-1)\theta_{p_f}}\right]^H, \tag{7}$$

where $\theta_{p_f} = \frac{\beta}{\lambda} cos\left(\psi_{p_f}\right)$ and ψ_{p_f} correspond to the actual physical angles of the p_f-th far-field path, and $\beta = \frac{\lambda}{2}$ is the distance between adjacent antennas.

Since the far-field channel is non-sparse, this may introduce a huge pilot overhead in channel estimation. Therefore, we need to use the DFT matrix $\mathbf{A}$ to transform $\mathbf{h}_{FF}$ into a sparse angular domain channel $\mathbf{h}_{FF}^A$, which can be represented as:

$$\mathbf{h}_{FF} = A\mathbf{h}_{FF}^A, \tag{8}$$

where $\mathbf{A} = [\mathbf{a}(\vartheta_1), \cdots, \mathbf{a}(\vartheta_N)] \in \mathbb{C}^{N\times N}$ ($\vartheta_n = \frac{2n-N-1}{N} n = 1, \cdots, N$) is an unitary matrices. It is worth noting that $\mathbf{h}_{FF}^A$ is the sparse representation of the far-field channel $\mathbf{h}_{FF}$ in the angular domain.Therefore, we can use CS algorithms to further reduce the pilot overhead of the channel.

In addition, the near-field channel $\mathbf{h}_{NF}$ can be modeled as follows:

$$\mathbf{h}_{NF} = \sqrt{\frac{N}{P}} \sum_{p_n=1}^{P_N} \mu_{p_n} \mathbf{b}(\theta_{p_n}, l_{p_n}), \tag{9}$$

where $P_N, \mu_{p_n}, \theta_{p_n}$ and l_{p_n} represent the total number of paths, path gains, actual physical path angles, and distances between thep_n-th scatterer and the uniform linear array antennas respectively. $\mathbf{b}(\theta_{p_n}, l_{p_n}) \in \mathbb{C}^{N\times 1}$ is the steering vector of the near-field array, which can be represented as:

$$\mathbf{b}(\theta_{p_n}, l_{p_n}) = \frac{1}{\sqrt{N}} \left[e^{-j\frac{2\pi}{\lambda}(l_{p_n}^{(1)} - l_{p_n})}, \cdots, e^{-j\frac{2\pi}{\lambda}(l_{p_n}^{(N)} - l_{p_n})}\right]^H, \tag{10}$$

where $l_{p_n}^{(n)} = \sqrt{l_{p_n}^2 - 2l_{p_n}\zeta\beta\theta_{p_n} + \beta^2\zeta^2}$ refers to the distance between the p_n-th scatterer and the $n-$th antenna of the base station. The transformation matrix in polar coordinate domain can be represented as $\mathbf{D}$:

$$\mathbf{D} = \left[\mathbf{b}\left(\theta_1, l_1^1\right), \cdots, \mathbf{b}\left(\theta_1, l_1^{Z_1}\right), \cdots, \mathbf{b}\left(\theta_N, l_N^{Z_N}\right)\right], \tag{11}$$

where θ_n and $l_n^{\zeta_n}$ respectively represent the sampled physical angle and the distance between the scatterer and the $n-$th antenna of the base station. The near-field channel model can be represented as follows:

$$\mathbf{h}_{NF} = \mathbf{D}\mathbf{h}_{NF}^P, \tag{12}$$

where $\mathbf{h}_{NF}^P \in \mathbb{C}^{Z\times 1}$ is the sparse channel vector in polar coordinate domain, and the sparse property can further reduce the pilot overhead of channel estimation.

By combining the far-field and near-field channels, a hybrid-field channel model is introduced, which can be represented as follows:

$$\mathbf{h} = \sqrt{\frac{N}{P}} \left(\sum_{p_f=1}^{\epsilon P} \gamma_{p_n} \mathbf{a}(\theta_{p_f}) + \sum_{p_n=1}^{(1-\epsilon)P} \mu_{p_n} \mathbf{b}(\theta_{p_n}, l_{p_n})\right), \tag{13}$$

where ϵ represents the ratio of far-field channel paths and near-field channel paths. $p_f + p_n = P$ denote total number of paths for hybrid-field channel and $\epsilon \in [0, 1]$ is control variables. The hybrid-field channel model can be obtained through equations (8) and (12), and can be further described as follows:

$$\mathbf{h} = \mathbf{A}\mathbf{h}_{FF}^A + \mathbf{D}\mathbf{h}_{NF}^P. \tag{14}$$

Let $\mathbf{B}=\mathbf{\Phi A} \in \mathbb{C}^{\tau N_{RF}\times N}$ and $\mathbf{W}=\mathbf{\Phi D} \in \mathbb{C}^{\tau N_{RF}\times Z}$ respectively undergo channel estimation using CS algorithms, representing the sensing matrices of the far-field channel and the near-field channel. Therefore, (3) can be further represented as follows:

$$\begin{aligned} \overline{\mathbf{y}} &= \mathbf{\Phi A}\mathbf{h}_{FF}^A + \mathbf{\Phi D}\mathbf{h}_{NF}^P + \overline{\mathbf{w}} \\ &= \mathbf{B}\mathbf{h}_{FF}^A + \mathbf{W}\mathbf{h}_{NF}^P + \overline{\mathbf{w}} \\ &= \mathbf{S}\overline{\mathbf{h}} + \overline{\mathbf{w}}, \end{aligned} \tag{15}$$

where $\mathbf{S} = [\mathbf{B}, \mathbf{W}] = \mathbf{\Phi\Psi} \in \mathbb{C}^{\tau N_{RF}\times(Z+N)}$, $\mathbf{\Psi} = [\mathbf{A}, \mathbf{D}] \in \mathbb{C}^{N\times(Z+N)}$, $\overline{\mathbf{h}} = [\left(\mathbf{h}_{FF}^A\right)^H, \left(\mathbf{h}_{NF}^P\right)^H]^H \in \mathbb{C}^{(Z+N)\times 1}$. Therefore, this paper no longer estimates the near-field or far-field channel separately, but adopts joint estimation of the hybrid-field channel, which enables a more efficient estimation of the hybrid-field channel. Subsequently, we focus solely on equation (15) to propose algorithm design solutions.

III. THE PROPOSED SWOMP CHANNEL ESTIMATION METHOD FOR JOINT HYBRID-FIELD CHANNEL ESTIMATION

In this paper adopts the Simultaneous Weighted Orthogonal Matching Pursuit (SWOMP) algorithm, which can accurately estimate the hybrid-field channel even without knowing its sparsity. Due to the matrix inversion operation in the algorithm, an equivalent matrix inversion operation based on the ''Woodbury'' transformation is proposed. A detailed derivation process based on the ''Woodbury'' transformation is provided to demonstrate this. According to the compressive sensing theory, the problem of hybrid-field channel

estimation can be formulated as follows:

$$\hat{\bar{\mathbf{h}}} = \text{argmin}_{\bar{\mathbf{h}}} \|\bar{\mathbf{h}}\|_0 \quad \text{s.t.} \quad \|\bar{\mathbf{y}} - \mathbf{S}\bar{\mathbf{h}}\|_2^2 \leq \varrho, \tag{16}$$

where ϱ is a constant related to the noise level.

Formula (16) is a Compressed Sensing (CS) problem of a Single Measurement Vector (SMV). Since the sparsity of the channel is generally unknown in practical scenarios, the SWOMP algorithm is used to solve the hybrid-field channel estimation problem. Next, the algorithm is described in detail. Firstly, the received signal $\bar{\mathbf{y}}$, sensing matrix $\mathbf{S}$, and threshold δ are inputted, where δ is related to the variance of the noise σ_0^2. Then, since the sparsity of the channel is unknown, a while loop is used. In the first step of the algorithm, the compressed sensing matrix is multiplied by the defined residual vector $\mathbf{r}$. In the second step, the position of the maximum value in the multiplied vector is found, which corresponds to the column number of the sensing matrix. In the third step, a support set is formed from the selected columns of the sensing matrix in each loop. In the fourth step, the pseudo-inverse of the support set is obtained, and then multiplied with the received signal $\bar{\mathbf{y}}$ to obtain an estimate of the hybrid-field channel. In the fifth step, the residual is updated. In the sixth step, the mean square error of the residual is calculated until it is less than the threshold δ. Where the threshold δ is derived based on prior information of the received signal [19], while the threshold used in [23] is chosen as an appropriate value to serve as the stopping criterion for the sparse recovery algorithm.and then the algorithm ends, completing the channel estimation. The specific **Algorithm 1** process is summarized as follows.

Algorithm 1 Proposed SWOMP Algorithm for Hybrid-Field Channel Estimation

Input: $\bar{\mathbf{y}}$, $\mathbf{\Phi}$, $\mathbf{A}$, $\mathbf{D}$, δ
Output: $\hat{\bar{\mathbf{h}}}$
Initialization: $\Omega = \emptyset$, $\mathbf{r} = \bar{\mathbf{y}}$, $T = size(\bar{\mathbf{y}}, 1)$.
// Joint estimate hybrid-field channel
1. $\mathbf{S} = [\mathbf{\Phi A}, \mathbf{\Phi D}]$
2. **While** RMSE $> \delta$ **do**
3. $c^* = \text{argmax} \left\|\mathbf{S}^H(:, n)\mathbf{r}\right\|_2^2, n = 1, 2, \cdots, (N + Z)$
4. $\Omega = \Omega \cup c^*$
5. $\hat{\bar{\mathbf{h}}} = (\mathbf{S}_\Omega)^\dagger \bar{\mathbf{y}}$
6. $\mathbf{r} = \bar{\mathbf{y}} - \mathbf{S}_\Omega \hat{\bar{\mathbf{h}}}$
7. RMSE $= \frac{1}{T} * \text{trace}\left(\mathbf{r}^H * \mathbf{r}\right)$
8. **end**

IV. THE PROPOSED WOODBURY SWOMP ALGORITHM

As can be seen from Algorithm 1, there is a step involving matrix inversion. Therefore, we propose an equivalent matrix inversion operation based on the "Woodbury" transformation.

The mathematical expression of the "Woodbury" transform can be written as

$$\left(\bar{\bar{\mathbf{A}}}^H \bar{\bar{\mathbf{A}}} + \varsigma \mathbf{I}\right)^{-1} = \frac{1}{\varsigma}\left(\mathbf{I} - \bar{\bar{\mathbf{A}}}^H \left(\varsigma \mathbf{I} + \bar{\bar{\mathbf{A}}}\bar{\bar{\mathbf{A}}}^H\right)^{-1} \bar{\bar{\mathbf{A}}}\right),$$

where ς represents a tunable parameter. Therefore, we transform the matrix inversion operation in the algorithm into this form of the Woodbury transform. Since the matrix $\bar{\bar{\mathbf{A}}}$ to be transformed contains complex numbers, we further discuss the transformation for various scenarios to adapt to this form of transformation. Then, Step 5 of the algorithm can be further expanded as follows:

$$\hat{\bar{\mathbf{h}}} = (\mathbf{S}_\Omega)^\dagger \bar{\mathbf{y}} = \left(\mathbf{S}_\Omega^H \mathbf{S}_\Omega\right)^{-1} \mathbf{S}_\Omega^H \bar{\mathbf{y}}, \tag{17}$$

where $\dagger$ represents the pseudo-inverse of the matrix, and $\mathbf{S}_\Omega$ represents a matrix set composed of column vectors selected from the sensing matrix $\mathbf{S}$ in each loop of the SWOMP algorithm. The number of columns in matrix $\mathbf{S}_\Omega$ is related to the sparsity of the hybrid-field channel. $\left(\mathbf{S}_\Omega^{\mathrm{H}} \mathbf{S}_\Omega\right)^{-1}$ represents the inverse of matrix $\mathbf{S}_\Omega^H \mathbf{S}_\Omega$, and H represents the conjugate transpose. In order to conform to the Woodbury transformation, $\left(\mathbf{S}_\Omega^H \mathbf{S}_\Omega\right)^{-1}$ needs to be transformed. Since the signal sent by the user is complex, the support set $\mathbf{S}_\Omega$ is a complex matrix, and let $\mathbf{X} = \mathbf{S}_\Omega^H \mathbf{S}_\Omega$, then $\mathbf{X}$ is a Hermitian matrix, that is, its diagonal elements are all real numbers. Therefore, $\mathbf{X}$ can be expressed as:

$$\mathbf{X} = \mathbf{U} + \text{diag}\left[\mathbf{e}_1, \cdots, \mathbf{e}_M\right], \tag{18}$$

where matrix $\mathbf{U}$ represents the non-diagonal elements of matrix $\mathbf{X}$, diag represents the diagonalization operation, $[\mathbf{e}_1, \cdots, \mathbf{e}_M]$ is a row vector, and $(\mathbf{e}_m,\ m = 1, 2, \cdots, M)$ represents the diagonal elements of matrix $\mathbf{X}$. Formula (18) can also be written as:

$$\mathbf{X} = \mathbf{U}_1 + \alpha \mathbf{I}_M. \tag{19}$$

In this case, let α represent the assigned coefficients and $\mathbf{I}_M$ represent the $M \times M$ identity matrix. Based on equation (19), in order to satisfy the form of the Woodbury transformation, which is an identity matrix multiplied by the coefficient α and then added with an unknown matrix $\mathbf{U}_1$, equaling the original matrix $\mathbf{X}$, we only need to analyze the diagonal elements of matrix $\mathbf{U}_1$. If a diagonal element of matrix $\mathbf{X}$ is greater than α, then the corresponding diagonal element of matrix $\mathbf{U}_1$ should be subtracted byα. If a diagonal element of matrix $\mathbf{X}$ is smaller than α, then the corresponding diagonal element of matrix $\mathbf{U}_1$ should be equal to α minus the value of the corresponding diagonal element in matrix $\mathbf{X}$, but with the opposite sign. This way, we obtain the values of the diagonal elements of matrix $\mathbf{U}_1$. The non-diagonal elements of matrix $\mathbf{U}_1$ are the same as the non-diagonal elements of matrix $\mathbf{X}$. Through the above analysis, it can be concluded that $\mathbf{U}_1$ is also a Hermitian matrix. Therefore, the unknown matrix $\mathbf{U}_1$ has been determined.To further conform to the form of the Woodbury transformation, it is necessary to

further decompose matrix $\mathbf{U}_1$ into the product of its conjugate transpose and an identical matrix. Therefore, the next step is to explain how matrix $\mathbf{U}_1$ can be decomposed in order to achieve this form. Performing an eigenvalue decomposition on matrix $\mathbf{U}_1$ will yield the solution.

$$\mathbf{U}_1 = \overline{\mathbf{A}}\mathbf{E}\overline{\mathbf{A}^{\mathrm{H}}}, \tag{20}$$

where $\overline{\mathbf{A}}$ is an orthogonal matrix, and $\mathbf{E}$ is a diagonal matrix with its diagonal elements being the eigenvalues of matrix $\mathbf{U}_1$. Next, let's analyze how to decompose matrix $\mathbf{U}_1$ into the product of a matrix and its transpose. (The eigenvalues of a Hermitian matrix are real numbers). Next, we will analyze several scenarios based on the ''Woodbury'' transform and then summarize the final conclusions.

In the first case, if all eigenvalues of matrix $\mathbf{U}_1$ are non-negative real numbers, then decompose the eigenvalue matrix E of $\mathbf{U}_1$ to obtain:

$$\mathbf{E} = \sqrt{\tilde{\mathbf{E}}\mathbf{I}_M}\sqrt{\tilde{\mathbf{E}}}\,, \tag{21}$$

where $\sqrt{\tilde{\mathbf{E}}}$ is also a diagonal matrix. Then, $\mathbf{U}_1$ can be expressed as:

$$\begin{aligned}\mathbf{U}_1 &= \overline{\mathbf{A}}\sqrt{\tilde{\mathbf{E}}\mathbf{I}_M}\sqrt{\tilde{\mathbf{E}}}\overline{\mathbf{A}^H} \\ &= (\overline{\mathbf{A}}\sqrt{\tilde{\mathbf{E}}})\mathbf{I}_M(\overline{\mathbf{A}}\sqrt{\tilde{\mathbf{E}}})^H \\ &= \mathbf{U}_2\mathbf{U}_2^H\,,\end{aligned} \tag{22}$$

where $\mathbf{U}_2 = \overline{\mathbf{A}}\sqrt{\tilde{\mathbf{E}}}$. The conjugate transpose of a non-negative number is still non-negative. In the second case, if all eigenvalues of matrix $\mathbf{U}_1$ are negative, then $\mathbf{E}$ can be expressed as:

$$\mathbf{E} = \sqrt{\tilde{\mathbf{E}}\mathbf{I}_M}\left(\sqrt{\tilde{\mathbf{E}}}\right)^H. \tag{23}$$

In this case, after taking the square root of a negative number, it becomes an imaginary number, thus we need to add a conjugate transpose. Therefore, $\mathbf{U}_1$ can be expressed as:

$$\begin{aligned}\mathbf{U}_1 &= \overline{\mathbf{A}}\sqrt{\tilde{\mathbf{E}}\mathbf{I}_M}\left(\sqrt{\tilde{\mathbf{E}}}\right)^H\overline{\mathbf{A}^H} \\ &= (\overline{\mathbf{A}}\sqrt{\tilde{\mathbf{E}}})\mathbf{I}_M(\overline{\mathbf{A}}\sqrt{\tilde{\mathbf{E}}})^H \\ &= \mathbf{U}_2\mathbf{U}_2^H.\end{aligned} \tag{24}$$

In the third case, if the eigenvalues of matrix $\mathbf{U}_1$ include both negative and positive numbers, then $\mathbf{E}$ can be expressed as:

$$\mathbf{E} = \sqrt{\tilde{\mathbf{E}}\mathbf{I}_M}\left(\sqrt{\tilde{\mathbf{E}}}\right)^H. \tag{25}$$

As we can see, it is the same as the second case. This is because the conjugate transpose of a positive number is still itself, thus adding the conjugate transpose does not have any effect. Therefore, $\mathbf{U}_1$ can be expressed as:

$$\begin{aligned}\mathbf{U}_1 &= \overline{\mathbf{A}}\sqrt{\tilde{\mathbf{E}}\mathbf{I}_M}\left(\sqrt{\tilde{\mathbf{E}}}\right)^H\overline{\mathbf{A}^H} \\ &= (\overline{\mathbf{A}}\sqrt{\tilde{\mathbf{E}}})\mathbf{I}_M(\overline{\mathbf{A}}\sqrt{\tilde{\mathbf{E}}})^H \\ &= \mathbf{U}_2\mathbf{U}_2^H.\end{aligned} \tag{26}$$

Based on the discussion of the three cases mentioned above, matrix $\mathbf{U}_1$ can be written in the form of a matrix multiplied by the transpose of another matrix. Therefore, let $\mathbf{Y} = \mathbf{U}_2^H$, then $\mathbf{Y}^H = \mathbf{U}_4$, and as a result, $\mathbf{X}$ can be written as:

$$\mathbf{X} = \mathbf{Y}^H\mathbf{Y} + \alpha\mathbf{I}_M. \tag{27}$$

Therefore, based on equation (27), $\left(\mathbf{S}_\Omega^{\boldsymbol{H}}\mathbf{S}_\Omega\right)^{-1}$ can be further expressed as:

$$\left(\mathbf{S}_\Omega^{\boldsymbol{H}}\mathbf{S}_\Omega\right)^{-1} = \left(\mathbf{Y}^{\boldsymbol{H}}\mathbf{Y} + \alpha\mathbf{I}_M\right)^{-1}. \tag{28}$$

Then, by employing the Sherman-Morrison-Woodbury formula, also known as the ''Sherman-Morrison-Woodbury'' transformation [20], abbreviated as the ''Woodbury'' transformation, Therefore, based on the aforementioned mathematical form of the Woodbury transform, equation (28) can be written as:

$$\begin{aligned}\left(\mathbf{S}_\Omega^{\boldsymbol{H}}\mathbf{S}_\Omega\right)^{-1} &= \left(\mathbf{Y}^{\boldsymbol{H}}\mathbf{Y} + \alpha\mathbf{I}_M\right)^{-1} \\ &= \frac{1}{\alpha}\left(\mathbf{I}_M - \mathbf{Y}^H\left(\alpha\mathbf{I}_M + \mathbf{Y}\mathbf{Y}^H\right)^{-1}\mathbf{Y}\right).\end{aligned} \tag{29}$$

Finally, substituting the transformed equation (29) into equation (17), The channel estimation values we obtained for the mixed-field are as follows:

$$\hat{\mathbf{h}} = \frac{1}{\alpha}\left(\mathbf{I}_{\mathrm{M}} - \mathbf{Y}^{\mathrm{H}}\left(\alpha\mathbf{I}_{\mathrm{M}} + \mathbf{Y}\mathbf{Y}^{\mathrm{H}}\right) - 1\mathbf{Y}\right)\mathbf{S}_\Omega^H\overline{\mathbf{y}}. \tag{30}$$

At this point, the computational complexity after the transformation is $\mathcal{O}(M^3)$, where M represents the number of columns in the support set, i.e., the number of columns in the support matrix. Finally, by replacing the fifth step in Algorithm 1 with equation (30), the Woodbury SWOMP algorithm is derived. Due to space constraints, further elaboration is omitted here.

V. THE PROPOSED LOW COMPLEXITY SWOMP ALGORITHM BASED ON THE "GAUSS-SEIDEL" METHOD

Based on the derivation in the previous section, it can be concluded that the ''Woodbury'' transformation also involves the process of matrix inversion, even after decomposition, where the dimensions of the matrix remain the same as the dimensions of the support set. Fortunately, we found that the matrix inversion operation in the fourth step of the SWOMP algorithm is actually obtained using the least squares (LS) algorithm. As is well known, LS is used to solve linear equations. Therefore, we can use the Gauss-Seidel method based on approximate iteration to reduce the computational complexity of directly computing the matrix inversion operation in the LS algorithm.

Firstly, the SWOMP algorithm is an improvement upon the OMP algorithm. Based on the properties of OMP, the estimated channel obtained from each iteration of the algorithm and the corresponding residual are orthogonal projection [24]. As a result, the obtained support sets are mutually orthogonal, indicating that the rank($\mathbf{S}_\Omega$) is equal to M, forming a column full-rank matrix. Furthermore, the solution for $\mathbf{S}_\Omega\bar{\mathbf{q}} = 0$ is unique, which means that $\bar{\mathbf{q}}$ is a zero vector of size $M \times 1$. Hence, for any non-zero vector $\bar{\mathbf{x}}$ of size $M \times 1$, we have the following relationship:

$$(\mathbf{S}_\Omega\bar{\mathbf{x}})^H \mathbf{S}_\Omega\bar{\mathbf{x}} = \bar{\mathbf{x}}^H \left(\mathbf{S}_\Omega^H\mathbf{S}_\Omega\right)\bar{\mathbf{x}} = \bar{\mathbf{x}}^H\bar{\mathbf{L}}\bar{\mathbf{x}} > 0, \tag{31}$$

where the Gram matrix $\bar{\mathbf{L}} = {\mathbf{S}_\Omega}^H\mathbf{S}_\Omega$ is positive definite. Additionally, we have:

$$\bar{\mathbf{L}}^H = \left(\mathbf{S}_\Omega^H\mathbf{S}_\Omega\right)^H = \bar{\mathbf{L}}, \tag{32}$$

where $\bar{\mathbf{L}}$ is symmetric. Hence, $\bar{\mathbf{L}}$ is a symmetric positive semi-definite matrix. Due to this specific property and the presence of $\left(\mathbf{S}_\Omega^H\mathbf{S}_\Omega\right)^{-1}$ operation in equation (17), the "Gauss-Seidel" method can be efficiently utilized to address the high computational complexity caused by the matrix inversion operation in equation (17). This GS method can be used to solve the linear equation $\bar{\mathbf{A}}\tilde{\mathbf{k}} = \grave{\mathbf{c}}$, where $\bar{\mathbf{A}}$ is a symmetric positive definite matrix, $\tilde{\mathbf{k}}$ is a solution vector, and $\grave{\mathbf{c}}$ is an observation vector. Traditional methods directly compute $\bar{\mathbf{A}}^{-1}\grave{\mathbf{c}}$ to obtain $\tilde{\mathbf{k}}$; however, the GS method can effectively obtain the solution to this equation iteratively with lower complexity. Since the matrix $\bar{\mathbf{A}}$ is symmetric positive definite, we can decompose matrix $\bar{\mathbf{A}}$ into a strictly lower triangular matrix $\Xi_{\bar{\mathbf{A}}}$, a diagonal matrix $\ddot{\mathbf{D}}_{\bar{\mathbf{A}}}$, and a strictly upper triangular matrix $\Xi_{\bar{\mathbf{A}}}^H$.The operation of solving the linear equation $\bar{\mathbf{A}}\tilde{\mathbf{k}} = \grave{\mathbf{c}}$ based on the "Gauss-Seidel" method can be mathematically represented as [21]:

$$\tilde{\mathbf{k}}^{(i+1)} = \left(\ddot{\mathbf{D}}_{\bar{\mathbf{A}}} + \Xi_{\bar{\mathbf{A}}}\right)^{-1}\left(\grave{\mathbf{c}} - \Xi_{\bar{\mathbf{A}}}^H\tilde{\mathbf{k}}^{(i)}\right), i = 0, 1, 2\cdots \tag{33}$$

where i represents the number of iterations. In order to better conform to the form of solving linear iterations with GS as in (33), (17) can be rewritten:

$$\bar{\bar{\mathbf{L}}}\hat{\bar{\mathbf{h}}} = \bar{\bar{\mathbf{y}}} \tag{34}$$

where $\bar{\bar{\mathbf{y}}} = {\mathbf{S}_\Omega}^H\bar{\mathbf{y}}$ and $\hat{\bar{\mathbf{h}}} = \bar{\mathbf{L}}^{-1}\bar{\bar{\mathbf{y}}}$. Based on the above analysis, since the matrix $\bar{\mathbf{L}}$ is symmetric positive definite, it can be decomposed into:

$$\bar{\bar{\mathbf{L}}} = \bar{\bar{\mathbf{W}}} + \bar{\bar{\mathbf{\Xi}}} + \bar{\bar{\mathbf{W}}}^{\mathrm{H}}, \tag{35}$$

where $\bar{\bar{\mathbf{W}}}$, $\bar{\bar{\mathbf{\Xi}}}$ and $\bar{\bar{\mathbf{W}}}^H$ represent the strictly lower triangular matrix, diagonal matrix, and strictly upper triangular matrix, respectively. Based on the mathematical expression of the (33) GS method, the solution to problem (34) can be expressed as:

$$\hat{\bar{\mathbf{h}}}^{(i+1)} = \left(\bar{\bar{\mathbf{\Xi}}} + \bar{\bar{\mathbf{W}}}\right)^{-1}\left(\bar{\bar{\mathbf{y}}} - \bar{\bar{\mathbf{W}}}^H\hat{\bar{\mathbf{h}}}^{(i)}\right).\ \mathrm{i} = 0, 1, 2\cdots \tag{36}$$

Since $\bar{\bar{\mathbf{\Xi}}}+\bar{\bar{\mathbf{W}}}$ is a lower triangular matrix, $\hat{\bar{\mathbf{h}}}^{(i+1)}$ can be obtained through low-complexity computation, thus we have:

$$\hat{\bar{\mathbf{h}}}_{\bar{j}}^{(i+1)} = \frac{1}{\bar{\bar{\mathbf{L}}}_{\bar{j},\bar{j}}}\left(\bar{\bar{\mathbf{y}}}_{\bar{j}} - \sum\nolimits_{\bar{k}<\bar{j}}\bar{\mathbf{L}}_{\bar{j},\bar{k}}\hat{\bar{\mathbf{h}}}_{\bar{k}}^{(i+1)} - \sum\nolimits_{\bar{k}>\bar{j}}\bar{\mathbf{L}}_{\bar{j},\bar{k}}\hat{\bar{\mathbf{h}}}_{\bar{k}}^{(i)}\right), \tag{37}$$

where $\bar{j}, \bar{k} = 1, 2, \cdots, M$. $\hat{\bar{\mathbf{h}}}_{\bar{j}}^{(i)}$,$\hat{\bar{\mathbf{h}}}_{\bar{j}}^{(i+1)}$ and $\bar{\bar{\mathbf{y}}}_{\bar{j}}$ represent the $\bar{j}$-th element of $\hat{\bar{\mathbf{h}}}^{(i)}$,$\hat{\bar{\mathbf{h}}}^{(i+1)}$ and $\bar{\bar{\mathbf{y}}}$, respectively. $\bar{\mathbf{L}}_{\bar{j},\bar{k}}$ represents the element in the $\bar{j}$-th row and $\bar{k}$-th column of matrix $\bar{\mathbf{L}}$.

Therefore, by utilizing the linear approximation iterative method in (37), each element in $\hat{\bar{\mathbf{h}}}^{(i+1)}$ can be computed, ultimately converging to the vector value $\hat{\bar{\mathbf{h}}}$, which corresponds to $\hat{\mathbf{h}}$ in (17). From (37), it can be seen that in the calculation of $\hat{\bar{\mathbf{h}}}^{(i+1)}$, multiplication is required M times. Since $\hat{\bar{\mathbf{h}}}^{(i+1)}$ has M elements, the total number of multiplications is M^2.Furthermore, the convergence speed of the linear approximation iterative method based on GS is faster compared to the method based on Neumann [25], and it also has lower computational complexity [26].As shown in Table 1, we compared the complexity of the proposed algorithm.

TABLE 1. Algorithm complexity.

Algorithm	Computational Complexity
Far-field OMP	$\mathcal{O}(N\tau N_{RF}P^3) + \mathcal{O}(N^2)$
Near-field OMP	$\mathcal{O}(Z\tau N_{RF}P^3) + \mathcal{O}(NZ)$
Hybrid-field OMP	$\mathcal{O}(N\tau N_{RF}(\varepsilon P)^3) + \mathcal{O}(Z\tau N_{RF}((1-\varepsilon)P)^3) + \mathcal{O}(NZ)$
SWOMP	$\mathcal{O}\left((N+Z)\tau N_{RF}N_s^3\right) + \mathcal{O}\left(N(N+Z)\right)$
WD-SWOMP	$\mathcal{O}\left((N+Z)\tau N_{RF}N_s^3\right) + \mathcal{O}\left(N(N+Z)\right)$
LC-SWOMP	$\mathcal{O}\left((N+Z)\tau N_{RF}(iN_s^2)\right) + \mathcal{O}((N+Z)N)$

Here, N_s represents the adaptively hybrid-field sparsity level in the SWOMP algorithm. $i$represents the total number of iterations for the GS approximate iteration.It can be observed that the complexity of the algorithm is concentrated on N_s^3, therefore reducing it to a square will result in a significant decrease in complexity. Similarly, by replacing the approximate iterative convergence in Algorithm 1 with the fifth step, the LC-SWOMP algorithm is obtained.

VI. SIMULATION RESULTS AND PERFORMANCE ANALYSES OF THE PROPOSED SCHEME

In this section, we use several algorithms to compare the performance of the proposed algorithm. The compared algorithms include hybrid-Field OMP [14], Far-Field OMP [27], Near-Field OMP [10], and Minimum Mean Square Error (MMSE) algorithm. Additionally, we define Normalized

Mean Square Error (NMSE) as a metric for performance evaluation, which can be expressed as:

$$\mathrm{NMSE} = 10\log_{10}\frac{\|\mathbf{h}-\hat{\mathbf{h}}\|_2^2}{\|\mathbf{h}\|_2^2}, \tag{38}$$

where $\hat{\mathbf{h}} = \boldsymbol{\Psi}\hat{\tilde{\mathbf{h}}}$. Consider an uplink XL-MIMO communication system using hybrid beamforming. For the simulation parameters of the system, we employ a base station equipped with $N = 512$ antennas. The total number of path components is defined as $P = 6$. The number of radio frequency (RF) chains is set to $N_{RF} = 4$. The complex path gains for both near-field and far-field are defined as γ_{p_f}, μ_{p_n} $\mathcal{CN}(0, 1)$. The angles θ_{p_f} and θ_{p_n} correspond to θ_{p_f}, θ_{p_n} $\mathcal{U}(-1, 1)$. Additionally, the range of near-field distances is taken as $l_{p_n} = [10, 80]$ meters. For the polar domain transformation matrix $\mathbf{D}$, the number of sampling grids is Z=2071. In the XL-MIMO system, we only consider a single-carrier scenario. Thus, the carrier frequency is set to 30 GHz.

In Figure 2, the comparison of the NMSE performance between the proposed SWOMP algorithm and other algorithms is presented first. In this scenario, the adjustable parameter ϵ is set to 0.5, and the length of the pilot sequence is denoted as 64. From the graph, it can be observed that the proposed method exhibits higher accuracy in hybrid-field channel estimation. This is attributed to the joint estimation of both far-field and near-field hybrid channels, which reduces the error caused by initially estimating only the far-field channel and leads to improved performance. In addition, we can also observe that under high signal-to-noise ratio (SNR), the performance of the MMSE algorithm is superior to that of all other algorithms. This is because the pilot overhead required by the MMSE algorithm is equal to the number of base station antennas, and thus solving the linear problem is related to the SNR. As the SNR increases, the channel estimation error obtained by the MMSE algorithm becomes smaller. In our simulations, we only use the MMSE as a reference, and it can be seen that under low SNR, our proposed algorithm does not require pilot overhead consistent with the number of base station antennas, yet still outperforms the MMSE. This demonstrates the significant impact of the SNR on the MMSE algorithm in channel estimation and its requirement for high pilot overhead. Therefore, our proposed algorithm's effectiveness is further highlighted. As a result, the interpretations of Figures 3 and 4 follow a similar rationale, and will not be reiterated here.

As shown in Figure 3, the comparison mainly focuses on the proposed "Woodbury"-based transformed SWOMP algorithm and other algorithms. In this case, the adjustable parameter ϵ is set to 0.5, and the length of the pilot sequence is denoted as 64. From the graph, it can be observed that the algorithm after the "Woodbury" transformation almost completely overlaps with the traditional SWOMP algorithm in terms of NMSE performance. This indicates that the proposed "Woodbury"-based transformed SWOMP algorithm achieves the same level of accuracy as the matrix inversion approach, thus demonstrating the effectiveness of the proposed equivalent algorithm.

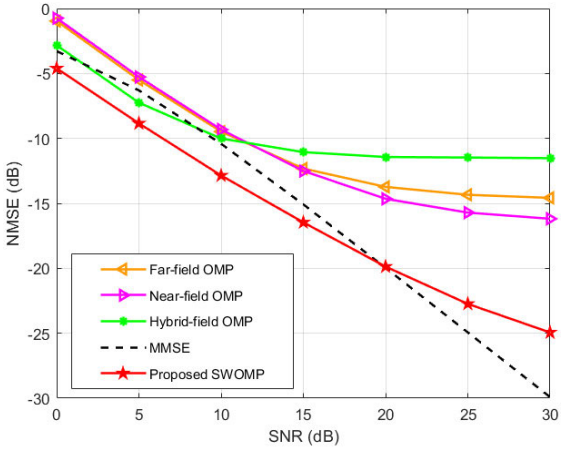

FIGURE 2. The proposed SWOMP is compared with NMSE under different signal-to-noise ratios.

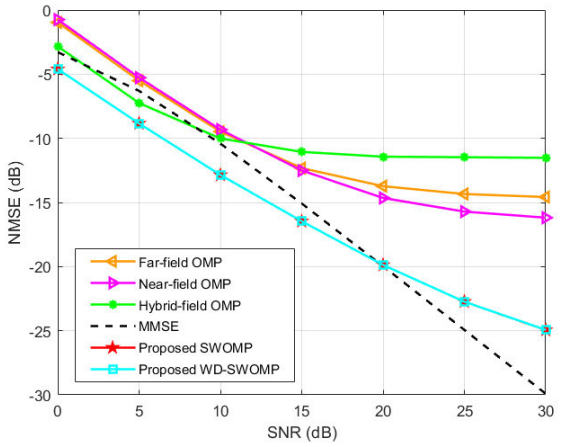

FIGURE 3. The two proposed algorithms are compared with NMSE under different SNR.

As shown in Figure 4, the performance of the proposed low-complexity SWOMP algorithm is compared with other algorithms. Similarly, the adjustable parameter ϵ is set to 0.5, and the length of the pilot sequence is denoted as 64. The low-complexity SWOMP (LC-SWOMP) algorithm after the "Gauss-Seidel" transformation eliminates the matrix inversion operation, and from the graph, it can be observed that its performance is almost identical to that of SWOMP and WD-SWOMP. This indicates that the proposed low-complexity algorithm not only maintains its performance but also has a certain reduction in computational complexity, thus demonstrating the effectiveness of the proposed algorithm.

As shown in Figure 5, the performance of the proposed SWOMP algorithm is compared with other algorithms under different path parameters ϵ. In this case, the adjustable parameter SNR is set to 5dB, and the length of the pilot sequence is set to 64. From the graph, it can be observed that

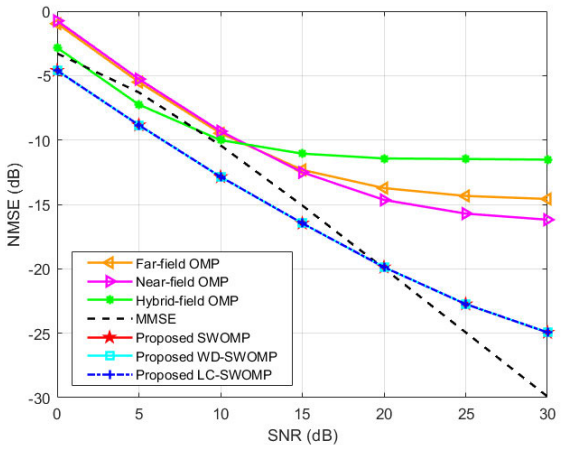

FIGURE 4. The proposed low complexity algorithm is compared with NMSE under different SNR.

the proposed algorithm outperforms other existing algorithms in terms of NMSE performance, and as the distance parameter ϵ increases, the NMSE continues to decrease. This is because as the parameter ϵ increases, the hybrid-field channel of the XL-MIMO system tends to favor the far-field channel, resulting in a dominant role of the far-field channel. The decreasing trend also indicates that the sparsity of the near-field channel is not as strong as that of the far-field channel. Therefore, compressed sensing algorithms perform better in channels with more obvious sparsity. When $\epsilon = 0$ and $\epsilon = 1$, the proposed SWOMP algorithm does not exhibit the NMSE performance of utilizing the OMP algorithm alone for channel estimation because it is based on the SWOMP algorithm. In the case of unknown channel sparsity, this algorithm can more accurately capture the sparsity of the channel, demonstrating better performance compared to traditional OMP algorithm.

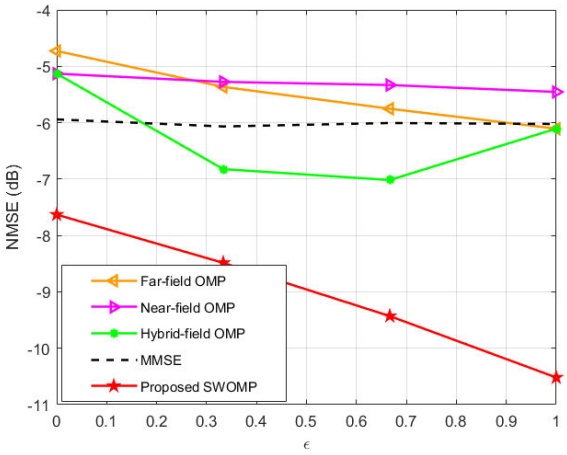

FIGURE 5. The proposed SWOMP is compared with NMSE under different path parameters.

To further demonstrate the superiority of the proposed algorithm based on the "Woodbury" equivalent transformation, we conducted comparisons between the proposed algorithm and the SWOMP algorithm under different channel parameters. The SNR was set to 5dB, and the pilot length was set to 64. From the Figure 6, it can be seen that the proposed algorithm does not sacrifice performance but rather overlaps almost perfectly with the performance curve of the SWOMP algorithm. This also indicates the effectiveness of the matrix inverse transformation based on the "Woodbury" method.

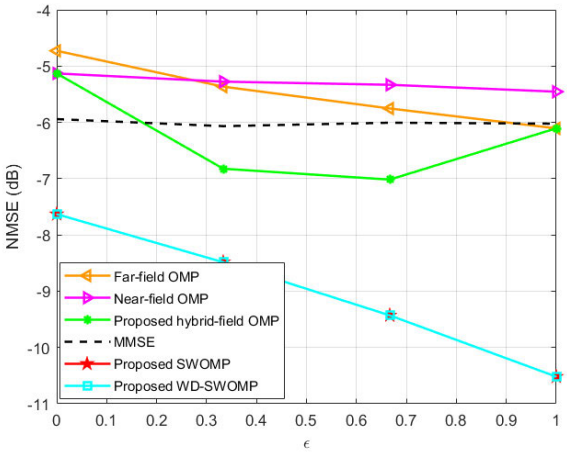

FIGURE 6. The two proposed algorithms are compared with NMSE under different path parameters.

In order to illustrate the comparison between the proposed LC-SWOMP algorithm and SWOMP, WD-SWOMP under different path parameters ϵ, we conducted another set of experiments as shown in Figure 7. In this simulation experiment, with SNR=5dB and pilot length of 64, it can be observed from the graph that the performance curve of the proposed LC-SWOMP algorithm almost overlaps with SWOMP and WD-SWOMP. This further demonstrates the good robustness of the proposed LC-SWOMP algorithm under different channel path parameters.

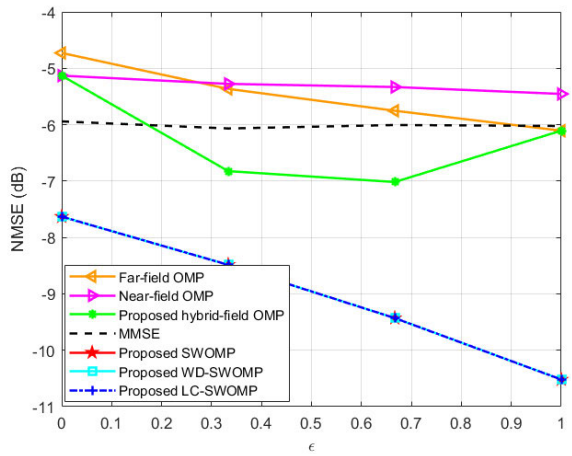

FIGURE 7. The proposed low complexity algorithm is compared with NMSE under different path parameters.

As shown in Figure 8, the performance comparison of the proposed SWOMP, WD-SWOMP, and LC-SWOMP algorithms under different pilot lengths is conducted in a simulation environment with SNR=0dB and path parameter ϵ=0.5. From the graph, it can be observed that the proposed SWOMP algorithm has better performance compared to other algorithms. The simulation curves of the proposed WD-SWOMP and LC-SWOMP almost overlap with the SWOMP, indicating that they have similar performance. This once again proves the effectiveness of the proposed WD-SWOMP and LC-SWOMP algorithms. Moreover, the proposed low-complexity SWOMP algorithm not only has comparable performance to the SWOMP algorithm but also reduces computational complexity. The simulation results demonstrate that this adaptive sparsity-based channel estimation method has certain effectiveness in hybrid-field channel estimation.

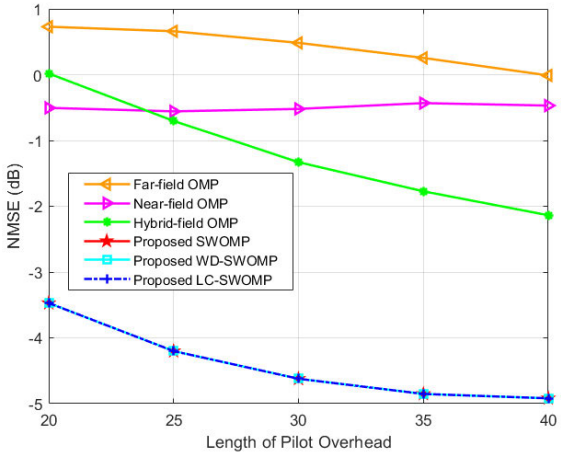

FIGURE 8. The performance comparison of the three proposed methods under different pilot lengths.

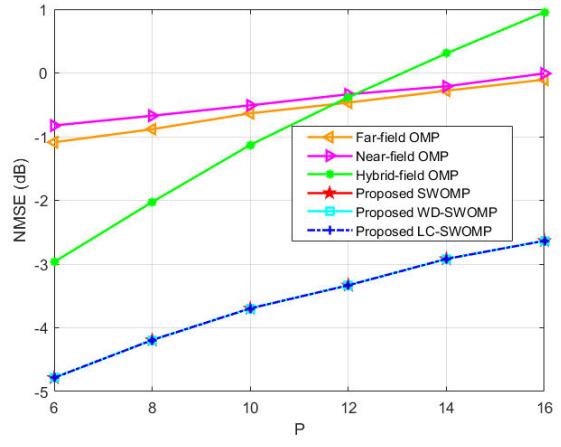

FIGURE 9. The performance comparison of the three proposed methods under different total number of paths.

As shown in Figure 9, a comparison between the proposed three methods and other hybrid-field channel estimation methods is conducted in a simulation environment with SNR=0dB and channel path parameter ϵ=0.5. From the graph, it can be observed that the proposed three methods have better performance compared to other methods. As the path parameter increases, the NMSE also increases, indicating that the estimated hybrid-field channel becomes less accurate. This is because as the number of paths increases, the non-sparse components of the channel also increase. Therefore, with an unchanged pilot length, compressive sensing faces some loss in estimation performance when dealing with channels with more non-sparse components. However, from the simulation graph, it can be seen that the proposed three methods consistently outperform other algorithms as the total number of paths increases. This once again proves the effectiveness of the proposed three methods in hybrid-field channel estimation.

VII. CONCLUSION

This article proposes a joint hybrid-field channel estimation scheme in XL-MIMO systems based on RF chain architecture. Based on the proposed approach using the SWOMP algorithm to address the problem in the presence of unknown channel sparsity, we found that the proposed algorithm can accurately obtain the hybrid-field channel state information. Subsequently, due to the matrix inversion operation in the SWOMP algorithm, we then proposed the WD-SWOMP algorithm based on the Woodbury transform for equivalent matrix inversion, which achieves the same channel estimation performance as the SWOMP algorithm. Furthermore, by employing linear approximate iteration to eliminate the matrix inversion step in the algorithm, we introduced the low-complexity LC-SWOMP algorithm. After iterative convergence, LC-SWOMP can achieve the same channel estimation performance. Finally, simulation results demonstrate the efficiency of the proposed hybrid-field channel estimation scheme and the effectiveness of the proposed algorithms.

REFERENCES

[1] W. Saad, M. Bennis, and M. Chen, "A vision of 6G wireless systems: Applications, trends, technologies, and open research problems," *IEEE Netw.*, vol. 34, no. 3, pp. 134–142, May 2020.

[2] Z. Zhang, Y. Xiao, Z. Ma, M. Xiao, Z. Ding, X. Lei, G. K. Karagiannidis, and P. Fan, "6G wireless networks: Vision, requirements, architecture, and key technologies," *IEEE Veh. Technol. Mag.*, vol. 14, no. 3, pp. 28–41, Sep. 2019.

[3] Z. Wang, J. Zhang, H. Du, W. E. I. Sha, B. Ai, D. Niyato, and M. Debbah, "Extremely large-scale MIMO: Fundamentals, challenges, solutions, and future directions," *IEEE Wireless Commun.*, early access, Apr. 10, 2023, doi: 10.1109/MWC.132.2200443.

[4] E. D. Carvalho, A. Ali, A. Amiri, M. Angjelichinoski, and R. W. Heath, "Non-stationarities in extra-large-scale massive MIMO," *IEEE Wireless Commun.*, vol. 27, no. 4, pp. 74–80, Aug. 2020.

[5] X. Gao, L. Dai, S. Han, C.-L. I, and R. W. Heath, "Energy-efficient hybrid analog and digital precoding for mmWave MIMO systems with large antenna arrays," *IEEE J. Sel. Areas Commun.*, vol. 34, no. 4, pp. 998–1009, Apr. 2016.

[6] Y. Huang, Y. He, W. He, L. Shi, T. Cheng, and Y. Sui, "Channel estimation in massive MIMO systems based on generalized block adaptive matching pursuit algorithm," *IEEE Wireless Commun. Lett.*, vol. 9, no. 12, pp. 2098–2101, Dec. 2020.

[7] M. Ke, Z. Gao, Y. Wu, X. Gao, and R. Schober, "Compressive sensing-based adaptive active user detection and channel estimation: Massive access meets massive MIMO," *IEEE Trans. Signal Process.*, vol. 68, pp. 764–779, 2020.
[8] Y. Mei, Z. Gao, Y. Wu, W. Chen, J. Zhang, D. W. K. Ng, and M. Di Renzo, "Compressive sensing-based joint activity and data detection for grant-free massive IoT access," *IEEE Trans. Wireless Commun.*, vol. 21, no. 3, pp. 1851–1869, Mar. 2022.
[9] M. Cui and L. Dai, "Near-field channel estimation for extremely large-scale MIMO with hybrid precoding," in *Proc. IEEE Global Commun. Conf. (GLOBECOM)*, Madrid, Spain, Dec. 2021, pp. 1–6.
[10] M. Cui and L. Dai, "Channel estimation for extremely large-scale MIMO: far-field or near-field?" *IEEE Trans. Commun.*, vol. 70, no. 4, pp. 2663–2677, Apr. 2022.
[11] M. Cui and L. Dai, "Near-field wideband channel estimation for extremely large-scale MIMO," *Sci. China Inf. Sci.*, vol. 66, no. 7, Jul. 2023, Art. no. 172303.
[12] H.-J. Song and T. Nagatsuma, "Present and future of terahertz communications," *IEEE Trans. Terahertz Sci. Technol.*, vol. 1, no. 1, pp. 256–263, Sep. 2011.
[13] J. Wu, S. Kim, and B. Shim, "Near-field channel estimation for RIS-assisted wideband terahertz systems," in *Proc. GLOBECOM IEEE Global Commun. Conf.*, Rio de Janeiro, Brazil, Dec. 2022, pp. 3893–3898.
[14] X. Wei and L. Dai, "Channel estimation for extremely large-scale massive MIMO: Far-field, near-field, or hybrid-field?" *IEEE Commun. Lett.*, vol. 26, no. 1, pp. 177–181, Jan. 2022.
[15] Y. Li and M. Jiang, "ADMM-based hybrid-field uplink channel estimation for extremely large-scale MIMO systems," in *Proc. IEEE/CIC Int. Conf. Commun. China (ICCC)*, Dalian, China, Aug. 2023, pp. 1–5.
[16] X. Peng, L. Zhao, Y. Jiang, J. Liu, and W. Li, "Channel estimation for extremely large-scale massive MIMO systems in hybrid-field channel," in *Proc. IEEE/CIC Int. Conf. Commun. (ICCC)*, Dalian, China, Aug. 2023, pp. 1–6.
[17] Z. Hu, C. Chen, Y. Jin, L. Zhou, and Q. Wei, "Hybrid-field channel estimation for extremely large-scale massive MIMO system," *IEEE Commun. Lett.*, vol. 27, no. 1, pp. 303–307, Jan. 2023.
[18] W. Yang, M. Li, and Q. Liu, "A practical channel estimation strategy for XL-MIMO communication systems," *IEEE Commun. Lett.*, vol. 27, no. 6, pp. 1580–1583, Jun. 2023.
[19] J. Rodríguez-Fernández, N. González-Prelcic, K. Venugopal, and R. W. Heath, "Frequency-domain compressive channel estimation for frequency-selective hybrid millimeter wave MIMO systems," *IEEE Trans. Wireless Commun.*, vol. 17, no. 5, pp. 2946–2960, May 2018.
[20] N. Parikh and S. Boyd, "Proximal algorithms," *Found. Trends Optim.*, vol. 1, pp. 127–239, Jan. 2014.
[21] A. Björck, *Numerical Methods for Least Squares Problems*. Philadelphia, PA, USA: Society for Industrial and Applied Mathematics, 1996.
[22] J. Tan and L. Dai, "Wideband channel estimation for THz massive MIMO," *China Commun.*, vol. 18, no. 5, pp. 66–80, May 2021.
[23] M. H. Bahonar, R. G. Zefreh, and R. Amiri, "Sparsity domain smoothing based thresholding recovery method for OFDM sparse channel estimation," in *Proc. 30th Int. Conf. Electr. Eng. (ICEE)*, Tehran, Iran, May 2022, pp. 720–725.
[24] J. A. Tropp, M. B. Wakin, M. F. Duarte, D. Baron, and R. G. Baraniuk, "Random filters for compressive sampling and reconstruction," in *Proc. IEEE Int. Conf. Acoust. Speed Signal Process.*, May 2006, p. 3.
[25] H. Prabhu, J. Rodrigues, O. Edfors, and F. Rusek, "Approximative matrix inverse computations for very-large MIMO and applications to linear precoding systems," in *Proc. IEEE Wireless Commun. Netw. Conf. (WCNC)*, Shanghai, China, Apr. 2013, pp. 2710–2715.
[26] X. Gao, L. Dai, J. Zhang, S. Han, and I. Chih-Lin, "Capacity-approaching linear precoding with low-complexity for large-scale MIMO systems," in *Proc. IEEE Int. Conf. Commun. (ICC)*, Jun. 2015, pp. 1577–1582.
[27] J. Lee, G.-T. Gil, and Y. H. Lee, "Channel estimation via orthogonal matching pursuit for hybrid MIMO systems in millimeter wave communications," *IEEE Trans. Commun.*, vol. 64, no. 6, pp. 2370–2386, Jun. 2016.

HUAN HUANG received the bachelor's degree from Henan University of Urban Construction, Pingdingshan, China, in 2021. He is currently pursuing the master's degree with the School of Information Science and Technology, Tibet University, Lhasa, Tibet, China. His research interests include sparse signal estimation and optimization algorithm design.

JUNXIN ZHANG is currently pursuing the master's degree with the School of Information Science and Technology, Tibet University, Lhasa, Tibet, China. His research interests include channel estimation, massive MIMO, millimeter-wave communications, and hybrid precoding.

JUN JIANG received the bachelor's degree in electronic and information engineering from Southwest University of Science and Technology, in 2003, and the master's degree in communication and information systems from Southwest Jiaotong University, in 2009. He is currently an Associate Professor with the School of Information Science and Technology, Tibet University. His research interests include sparse signal estimation and communication signal processing.